# Development of orthogonal tight-binding models for Ti-C and Ti-N systems

E. R. Margine,[1] A. N. Kolmogorov,[1] M. Reese,[2] M. Mrovec,[2] C. Elsässer,[2] B. Meyer,[3] R. Drautz,[4] and D. G. Pettifor[1]

[1]*Department of Materials, University of Oxford, Parks Road, Oxford OX1 3PH, United Kingdom*

[2]*Fraunhofer-Institute for Mechanics of Materials IWM, D-79108 Freiburg, Germany and IAM-ZBS, Karlsruhe Institute of Technology, D-76131 Karlsruhe, Germany*

[3]*Interdisciplinary Center for Molecular Materials (ICMM) and Computer Chemistry Center (CCC), Friedrich-Alexander Universität Erlangen-Nürnberg, D-91052 Erlangen, Germany*

[4]*Atomistic Modelling and Simulation, ICAMS, Ruhr-Universität Bochum, D-44801 Bochum, Germany*

(Received 4 July 2011; published 17 October 2011)

We develop *p-d* orthogonal tight-binding (OTB) models for the description of $TiC_x$ and $TiN_x$ compounds in the $1.0 > x > 0.5$ composition range. For the parametrization of bond integrals we use a recently developed method allowing projection of the one-electron wave functions obtained within the density functional theory onto optimized atom-centered orbitals. The performance of the OTB models is investigated for a wide range of properties: binding energy of elements and compounds, density of states, formation energy of vacancy-ordered defects, elastic constants, and phonon dispersions. The models provide a good description of the ground state properties at 1:1 composition and show a fair transferability for various atomic environments in elemental and binary phases.

DOI: 10.1103/PhysRevB.84.155120 PACS number(s): 62.20.−x, 71.15.Nc, 71.20.Be, 61.72.jd

## I. INTRODUCTION

Transition-metal carbides and nitrides (Ti-$X$, $X$ = C or N) are compounds of great technological importance due to their outstanding mechanical and physical properties.[1,2] They exhibit high hardness, high melting point, and excellent electrical and thermal conductivity.[1,2] This combination of properties is exploited in a variety of applications such as wear resistant coatings and cutting tools, thin films for electronic devices, and aerospace structural components.[1,2] In recent years, TiC- and TiN-based nanocomposites have emerged as candidates for superhard and ultrahard nanocoating materials and considerable effort has been devoted to their synthesis and characterization.[3–7]

The crystalline form of stoichiometric titanium carbide and nitride exists in the rock-salt (NaCl) structure. This structure displays deviations in stoichiometry over a wide range of concentrations $TiX_x$ (for $1.0 > x > 0.5$) due to the formation of vacancies on the nonmetal sublattice. Stable ordered defect structures crystallizing in periodic superlattices can be formed by annealing samples with a specific concentration of vacancies. In the case of $Ti_2C$, the existence of at least two vacancy-ordered structures, the cubic and trigonal forms, have been reported, but experimental and theoretical investigations do not agree on their relative stability at different temperatures.[8] On the other hand, $Ti_2N$ is found to crystallize in the tetragonal antirutile structure.[8]

Several experimental and theoretical techniques have been used to investigate the bonding, electronic, and mechanical properties of bulk crystals,[8–32] thin films,[33,34] surfaces,[29,30,35–39] and interfaces[3–7,29,40–43] of stoichiometric and substoichiometric Ti-C and Ti-N compounds. For example, x-ray photoemission,[9–13] high-resolution x-ray diffraction,[14] and electron energy-loss spectroscopy[16] were used to examine the effect of vacancy concentration on the electronic properties of $TiC_x$ and $TiN_x$. On the theoretical side, the effect of structural optimization on the atomic environment around vacancies and the electronic structure of substoichiometric $TiC_x$ was investigated using a combined approach of pseudopotential plane wave and full-potential linear muffin-tin orbital methods.[17,18] An orthogonal tight-binding model for titanium carbide developed by Tan *et al.*[26] was used to investigate variation in the lattice constant with the vacancy concentration,[26] surface relaxations,[44] and dissociation of dislocations.[45] Most recently, the interaction of point defects and their role on the thermal stability of TiC and TiN films[21,22] and the atomic structure of $TiN/Si_3N_4$ interfaces[42] were studied using density functional theory calculations.

Despite the success of the *ab initio* methods in providing an accurate and reliable description of the properties of materials at the atomic scale, their application is limited to system sizes of a few hundred atoms. To study dislocations, grain boundaries, interfaces, or nucleation and growth mechanisms large-scale molecular-dynamics simulations involving thousands of atoms are required. Thus, tight-binding models have been successfully used as a balance between very accurate but expensive *ab initio* methods and fast but less transferable empirical interatomic potentials. Although several tight-binding models were developed for the Ti-C system[10,25–28] and, to our knowledge, one for the Ti-N system,[25] no tests have been reported on their performance for phases other than the cubic one.

In this study we present two orthogonal tight-binding models for Ti-C and Ti-N compounds that have been optimized through a systematic fitting procedure. The models are capable of giving qualitatively correct results for a range of properties: density of states, binding energy, formation energy, elastic constants, and phonon dispersions. We have aimed to develop such orthogonal tight-binding (OTB) models that would be able to give an accurate description of several Ti-C and Ti-N phases and perform reasonably well for the elemental C, N, and Ti phases to be applicable to simulations of extended crystal defects or nucleation and growth processes.

The paper is organized as follows. In Sec. II, we present the tight-binding models and the parametrization of the bond

 

integrals and the repulsive interaction. Tests of the current models for density of states, binding energies, elastic constants, phonon dispersions, and formation energies of vacancy-ordered structures are discussed in Sec. III. A summary and concluding remarks are given in Sec. IV.

## II. METHODOLOGY

A transferable tight-binding model for $TiC_x$ or $TiN_x$ should be able to describe binary compounds in the whole composition range as well as the elemental phases. This is difficult to achieve due to the very different bonding mechanisms in the respective elemental ground states: a close-packed metallic Ti versus open covalent C/N structures. In the case of pure C/N, the electronic structure is characterized by strong hybridization between the $2s$ and $2p$ states. In the case of elemental Ti, the electronic structure consists of hybridized $sp$-$d$ states originating from the overlap of a narrow $d$ band and a broader, nearly free electron $sp$ band (most properties of transition metal alloys are well reproduced by OTB $d$ models in which the lack of the $s$ states is compensated by an adjustment of the number of the $d$ electrons, $N_d$). OTB models based only on the $p$ states of the nonmetal and the $d$ states of the metal have been traditionally used for the metal-carbide/nitride systems[26,46] because of the clear separation of the bands therein: The C-$2p$/N-$2p$ and Ti-$3d$ states form a wide band centered about the Fermi energy, the low-lying C-$2s$/N-$2s$ states do not contribute to the bonding, and the nearly free electron Ti-$sp$ states are located far above the Fermi level.[47]

With our primary focus on building a reliable model for $TiX_x$ *compounds*, we adopt the OTB $pd$ representation but monitor closely its performance for the elemental phases. One can expect that the reduction of the full $sp$ basis to just the $p$ set may lead to the model's spurious behavior for pure C and N; we show that a careful parameterization of the repulsive term ensures a fairly good description of the elemental binding energies. Similarly, the tuning of $N_d$ may affect the relative order of the closed-packed structures of pure Ti; we find that increasing $N_d$ from 2.2 to 3.0 results in an overall improved description of the binary ground states at an acceptable cost in errors incurred for the metal-rich compositions. Since the densities of states generated by these OTB $pd$ models for the crystalline Ti-C/Ti-N phases are confined to a single $pd$ band, the proposed parametrizations can be directly used in the future as a basis for analytic bond-order potentials.[48]

The two-center orthogonal tight-binding model approximates the binding energy of a system as a sum of three terms:

$$U = U_{\text{bond}} + U_{\text{prom}} + U_{\text{rep}}, \tag{1}$$

where $U_{\text{bond}}$, $U_{\text{prom}}$, and $U_{\text{rep}}$ are the attractive covalent bond energy, the promotion energy, and the repulsive energy, respectively [a detailed description of the tight-binding (TB) bond model formalism can be found in Ref. 49]. Since in our OTB model each element has only one type of orbital ($p$ for C/N and $d$ for Ti), the promotion energy term is equal to zero.

### A. Bond integrals

Bond integrals are crucial quantities in any TB model since they determine the band structure and, hence, the magnitude of the attractive bond energy. The bond integrals for our OTB models were obtained directly from density functional theory (DFT) calculations via a recently developed projection scheme.[50] This approach is based on constructing a minimal basis of optimized atomic orbitals that give the best possible representation of the electronic wave functions from self-consistent DFT calculations for selected reference structures. The main advantage of this procedure is that it avoids empirical fitting and instead provides a consistent, physically based set of parameters whose validity and range of applicability is known.

The orthogonal bond integrals necessary for our $p$-$d$ OTB model are displayed as functions of interatomic distance in Fig. 1. Different symbols correspond to different crystal structures used in the projection. The distance dependences were obtained by varying uniformly the volume of each structure. The results in Fig. 1 demonstrate a good transferability between different structures so that each bond integral can be represented well by a smooth continuous function of interatomic distance only and we adopt the functional form proposed by Goodwin, Skinner, and Pettifor (GSP):[51]

$$\beta(R) = \beta_0 \left(\frac{R_0}{R}\right)^n \exp\left\{n\left[-\left(\frac{R}{R_c}\right)^{n_c} + \left(\frac{R_0}{R_c}\right)^{n_c}\right]\right\}. \tag{2}$$

In order for the bond integrals $\beta(R)$ to go smoothly to zero at a specific cutoff distance, we take the third-order polynomial tail function introduced in Ref. 52:

$$t(R) = B_0 + B_1(R - R_1) + B_2(R - R_1)^2 + B_3(R - R_1)^3 \quad \text{for } R_1 < R < R_{\text{cut}}. \tag{3}$$

The coefficients are determined by requiring that $\beta(R)$ and $t(R)$ and their first derivative match at the joining point $R_1$, and that $t(R)$ and its first derivative become zero at the cutoff distance $R_{\text{cut}}$. For the convenience of molecular-dynamics simulations, the cutoff distance is chosen such that it goes to zero between first- and second-neighbor distance in the cases of C-C, N-N, and Ti-Ti and in the region of second-neighbor distance in the cases of Ti-C and Ti-N. We observed that higher cutoff values led to a poor agreement between the OTB and local-density approximation (LDA) for the binding curves in pure C and N and for the elastic constants for the compounds. The distance dependence of the bond integral as a function of separation is shown in Fig. 1 and the full set of parameters is given in Table I.

In Fig. 2, the band structures and the density of states (DOS) obtained from the present OTB parameters for TiC and TiN in the NaCl structure are compared with the results from density functional theory calculations. The DFT results were obtained using the projected augmented waves (PAW) method[53] within the LDA[54] as implemented in the VASP code.[55] A cutoff energy of 500 eV and dense Monkhorst-Pack[56] $k$ meshes were chosen to ensure numerical convergence. Overall, the main features of the LDA-DOS in the $p$-$d$ band are well reproduced (since the carbon/nitrogen $2s$-orbital is not present in the OTB model the corresponding low energy band is absent). In TiC the Fermi level lies at the minimum of the pseudogap that separates bonding from antibonding states, the additional valence electron in TiN causes the Fermi energy to rise above this minimum. The OTB models correctly reflect

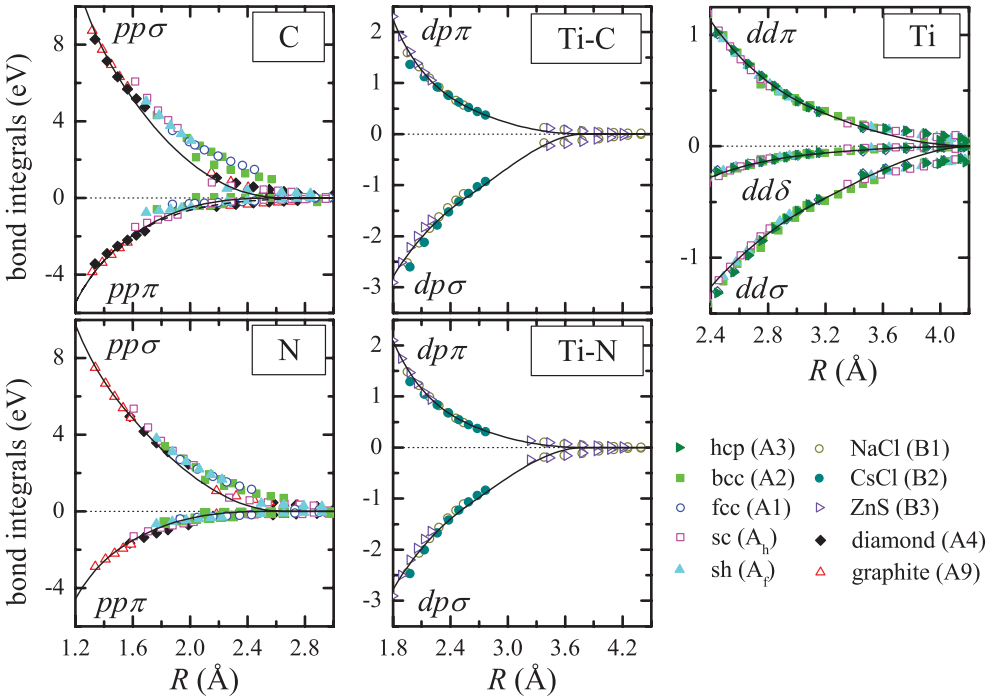


FIG. 1. (Color online) The distance dependence of the OTB bond integrals as a function of separation. The full lines represent the GSP functions [Eq. (2)] with the cutoff tail [Eq. (3)]. The LDA projection data are shown as symbols. The equilibrium nearest-neighbor bond length $R_0$ is given in Table I.

these features which are important for describing the electronic properties of these materials.

### B. Repulsive energy

The repulsive energy in our model is given by

$$U_{\text{rep}} = \sum_i f\left[\sum_{j\neq i}\phi(r_{ij})\right], \tag{4}$$

where the embedding functional $f$ is expressed as

$$f(x) = x^{n_1} + c_0 \tag{5}$$

and the repulsive pair potential takes the GSP form

$$\phi(R) = \phi_0\left(\frac{R_0}{R}\right)^n \exp\left\{n\left[-\left(\frac{R}{R_c}\right)^{n_c} + \left(\frac{R_0}{R_c}\right)^{n_c}\right]\right\}. \tag{6}$$

In order for the repulsive potential $\phi(R)$ to go smoothly to zero at a specific cutoff distance, we adopt the same tail function (3) as for the bond integrals. The repulsive potential parameters are determined by fitting the binding energy versus volume curves for selected structures of elemental and binary systems. For each structure we calculated the binding energy at 11 volume points including the equilibrium volume. The fitting database of total energies was obtained using the projected augmented waves method[53] within the local-density approximation[54] as described in the previous section.

TABLE I. The bond parameters for the GSP function $\beta(R)$ obtained from the LDA projection data shown in Fig. 1.

| | | $\beta_0$(eV) | $R_0$(Å) | $R_c$(Å) | $n$ | $n_c$ | $R_1$(Å) | $R_{\text{cut}}$(Å) |
|---|---|---|---|---|---|---|---|---|
| C | $pp\sigma$ | 6.1512 | 1.5120 | 2.6459 | 2.4916 | 6.6430 | 1.5200 | 2.6500 |
| | $pp\pi$ | −2.4631 | 1.5120 | 2.6459 | 2.5992 | 3.5708 | 1.5200 | 2.6500 |
| Ti-C | $pd\sigma$ | −1.9265 | 2.1481 | 2.9105 | 1.1275 | 1.7019 | 2.6000 | 3.8000 |
| | $pd\pi$ | 1.1411 | 2.1481 | 2.9105 | 2.1520 | 1.2576 | 2.6000 | 3.8000 |
| Ti | $dd\sigma$ | −0.8373 | 2.7460 | 2.9105 | 1.0949 | 2.3908 | 3.1751 | 4.2334 |
| | $dd\pi$ | 0.6322 | 2.7460 | 2.9105 | 1.7416 | 1.8335 | 3.1751 | 4.2334 |
| | $dd\delta$ | −0.1433 | 2.7460 | 2.9105 | 2.1189 | 1.6182 | 3.1751 | 4.2334 |
| Ti-N | $pd\sigma$ | −1.9253 | 2.1231 | 2.9105 | 1.1626 | 2.0600 | 2.6000 | 3.8000 |
| | $pd\pi$ | 1.0981 | 2.1231 | 2.9105 | 2.1755 | 1.3523 | 2.6000 | 3.8000 |
| N | $pp\sigma$ | 1.8376 | 2.1562 | 2.9105 | 2.2101 | 5.8212 | 1.5200 | 2.6500 |
| | $pp\pi$ | −0.3132 | 2.1562 | 2.9105 | 3.3261 | 4.8412 | 1.5200 | 2.6500 |

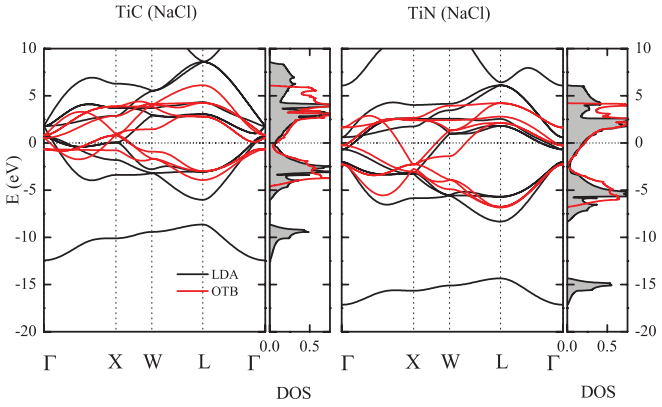


FIG. 2. (Color online) The electronic band structures and the density of states for TiC and TiN in the NaCl structure calculated using the present OTB model (red lines) are compared with the LDA calculations (black lines). The Fermi energy is taken as zero of energy and the density of states is given in units of states/(spin eV atom).

We start with the parametrization of the repulsive potential for the elemental phases. For elemental C we consider eight different structures with coordinations ranging from 1 to 14: dimer, linear chain (l-chain), graphite (A9), diamond (A4), simple cubic (sc, $A_h$), $\beta$-tin (A5), face-centered cubic (fcc, A1), and body-centered cubic (bcc, A2). Although in our OTB model the carbon atoms are characterized by only their valence $p$ electrons, the valence $s$ electrons play a critical role in providing the necessary repulsion to counter the attractive bond term. We find that the absence of the $s$-orbitals results in the unphysical stabilization of the dimer over the graphite ground state. This is not unexpected since the dimer coordination (of 1) is most different from the much higher values (from 2 to 14) in the other considered structures and our simple model could not properly account for the environment-dependent effects. A similar issue has been previously discussed in the case of titanium dimers.[57] To resolve this problem, an "ad hoc" short-range core correction term is introduced at small distances only for the dimer[48] (the expression for the correction term is given in the Appendix). Overall, the tight-binding energy curves as a function of the nearest-neighbor distance match well the *ab initio* results (Fig. 3) for carbon in $sp$, $sp^2$, and $sp^3$ bonding states although our basis set consists of only $p$ orbitals.

Under ambient conditions nitrogen forms $N_2$ molecules that at high pressure are compressed into compact covalent polymeric networks in which the strong triple molecular bonds evolve into single bonds.[58,59] To take into account the varieties of structures that nitrogen forms, the fitting database for elemental nitrogen includes: dimer, three chain structures [linear, armchair (a-chain), and zigzag (z-chain)], cubic gauche (cg) polymeric phase, and six bulk phases [diamond, simple cubic, face-centered cubic, body-centered cubic, simple hexagonal (sh, $A_f$), and hexagonal close-packed (hcp, A3)]. In analogy to the carbon model, only the $p$ orbitals are retained to define the bond energy and a short-range core

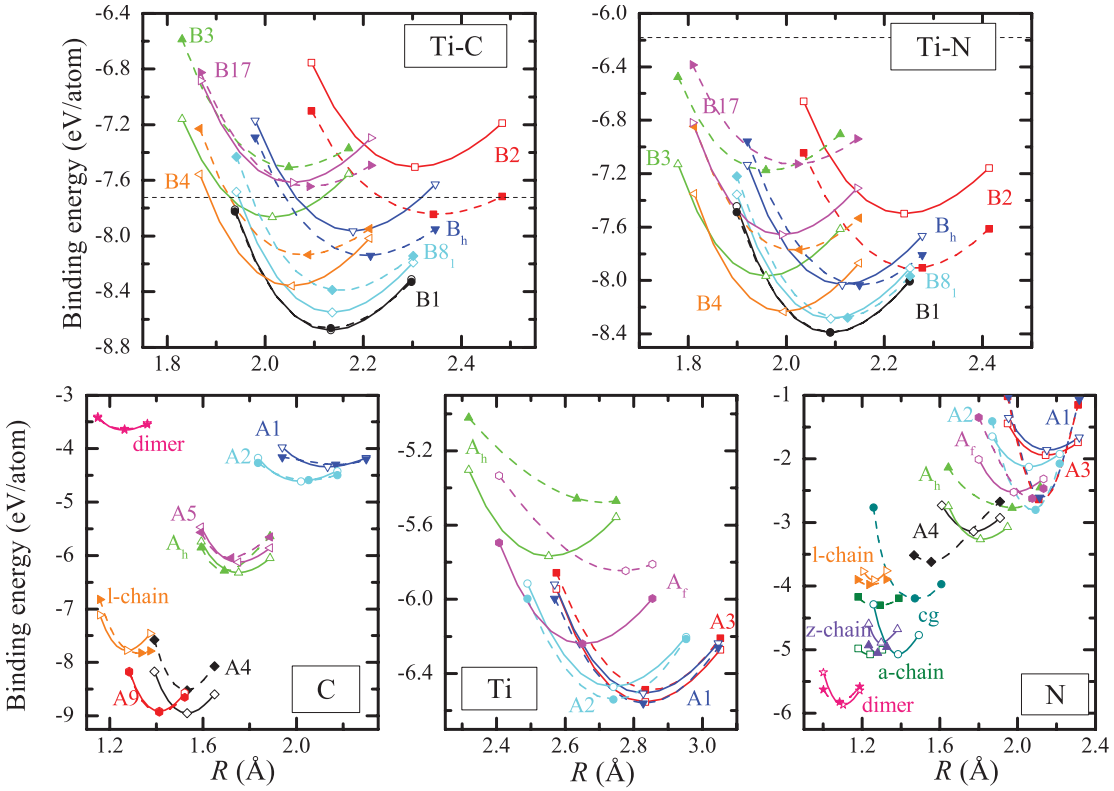


FIG. 3. (Color online) Bottom: binding energy as a function of interatomic nearest-neighbor distance for C (left panel), Ti (middle panel), and N (right panel). Top: binding energy as a function of interatomic distance for TiC and TiN at 1:1 composition (left and right panels). The dashed lines in the upper panels represent the zero formation energy. Open symbols connected by full lines represent the target LDA data and closed symbols connected by dashed lines represent the OTB result.

TABLE II. The parameters for the repulsive potential obtained from the fitting of the LDA binding curves shown in Fig. 3.

| | $\phi_0$(eV) | $R_0$(Å) | $R_c$(Å) | $n$ | $n_c$ | $R_1$(Å) | $R_{\text{cut}}$(Å) | $n_1$ | $c_0$(eV) |
|---|---|---|---|---|---|---|---|---|---|
| C | 10.7482 | 1.5400 | 2.5358 | 5.0684 | 9.3610 | 2.3200 | 2.5800 | 0.7322 | −3.3820 |
| Ti-C | 1.6359 | 2.1330 | 2.0538 | 5.8491 | 0.3257 | 2.6000 | 2.9000 | | |
| Ti | 0.2596 | 2.8334 | 1.5955 | 0.3134 | 4.2406 | 3.2000 | 3.5800 | 0.7732 | −2.4909 |
| Ti-N | 0.6940 | 2.0895 | 2.8477 | 6.6321 | 7.9922 | 2.6000 | 2.9000 | | |
| N | 1.7049 | 1.7700 | 2.2592 | 4.2518 | 12.9772 | 2.4000 | 2.6000 | 0.9129 | 1.0304 |

correction is used for the dimer. In contrast to the case of carbon, the sign of the fitted coefficient $\alpha$ is found to be negative (see the Appendix). This illustrates that the added term should not be considered as a core repulsion but rather a dimer correction allowing us to use the simple repulsive expression in Eq. (3) for the description of the wide range of coordinations and distances. This ensures that the dimer is the most stable structure and that none of the polymeric or bulk phases of nitrogen becomes erroneously the ground state (Fig. 3).

For the elemental Ti, five structures are included in the fitting database: simple cubic, face-centered cubic, body-centered cubic, simple hexagonal, and hexagonal close-packed. The main difficulty in developing an OTB model for titanium transferable from unary to binary phases originates in the varying number of $d$ electrons. According to the structural energy difference theorem[60] and in agreement with previous tight-binding models for titanium,[61,62] we obtain the correct relative ordering of the fcc and bcc phases with respect to the ground-state hcp structure when the number of electrons in the $d$ band is between $N_d = 2$ and $N_d = 2.2$. On the other hand, for TiC and TiN the theorem predicts the correct NaCl ground-state structure for a filling of the hybridized $p$-$d$ band of six and seven electrons, respectively. When going from elemental titanium to titanium carbide and nitride, the titanium $sp$ states are pushed up in energy by the nonmetal $s$ states beyond the hybridized $p$-$d$ band and about one electron is effectively transferred from the metallic $sp$ states to the $d$ states.[47] As we are primarily interested in describing formation energies of the binary systems and we have chosen to follow the approach used in Ref. 62 (for TiAl) rather than in Ref. 26 (for TiC), we set $N_d$ to 3.0 and keep it constant for the whole composition range. This choice affects the energy ordering of the lowest energy states for pure Ti (Fig. 3) [the Ti-hcp phase is 56 (31) meV/atom above fcc (bcc) compared to 47 (82) meV/atom below fcc (bcc) in the LDA] but introduces small errors in the formation energies for the binary phases.

To conclude our discussion on elemental phases, we note that our OTB models for C, N, and Ti are only meant to be used for Ti-C/Ti-N binary systems. Improved elemental tight-binding models will require the bond energy contribution coming from both $s$ and $p$ valence electrons rather than only the $p$ contribution in the case of C/N and the consideration of an appropriate number of $d$ electrons in the case of Ti.

Finally, keeping the elemental C-C/N-N and Ti-Ti repulsive potentials fixed, the Ti-C/Ti-N repulsive pair potentials are constructed using seven structure types at 1:1 composition: B1(NaCl), B2(CsCl), B3(ZnS), B4(ZnS), $B8_1$(NiAs),

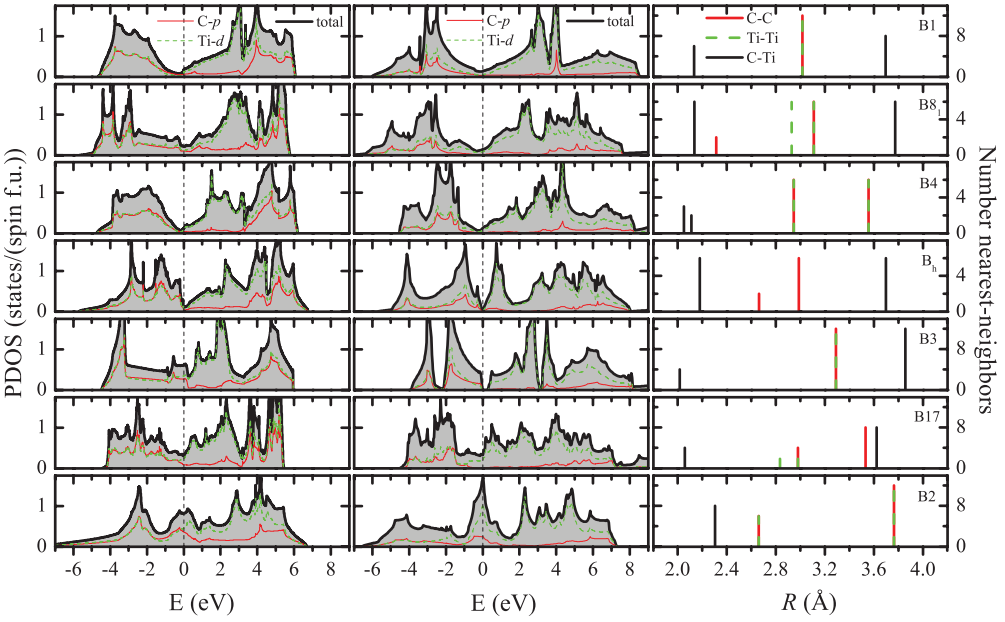


FIG. 4. (Color online) Projected density of states for TiC structures at 1:1 composition calculated using the present OTB model (left panel) and compared with the LDA calculations (middle panel). Fermi energy is taken as zero of energy. Number of nearest neighbors as a function of distance (right panel).

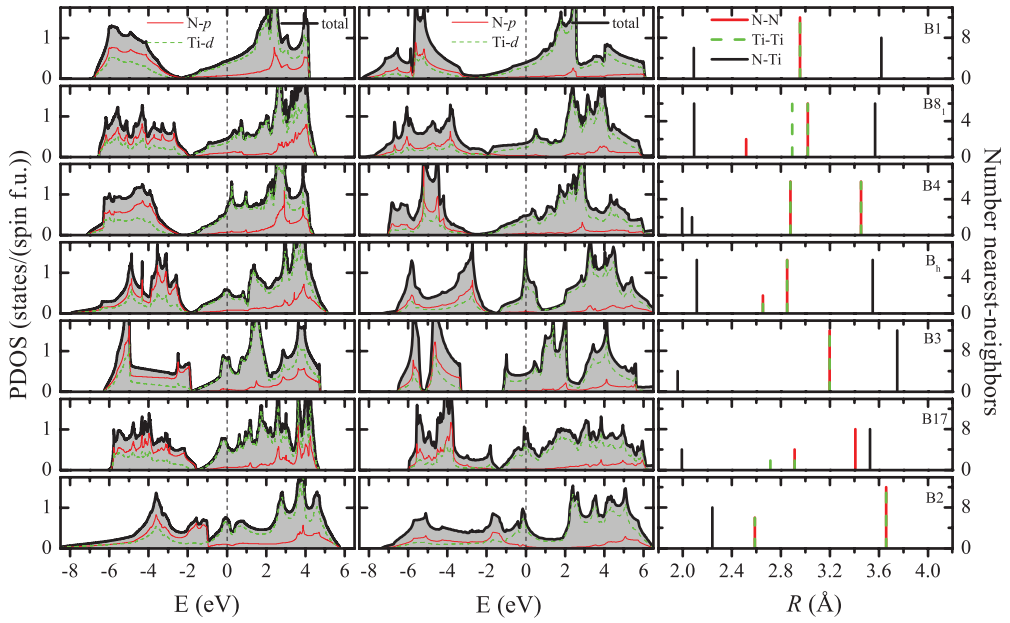


FIG. 5. (Color online) Projected density of states for TiN structures at 1:1 composition calculated using the present OTB model (left panel) and compared with the LDA calculations (middle panel). Fermi energy is taken as zero of energy. Number of nearest neighbors as a function of distance (right panel).

$B_h$(WC), and B17(PtS). The fitting is done with more weight on the lowest energy NaCl structure. The two upper panels in Fig. 3 present the total-energy curves as a function of the nearest-neighbor distance for the various structures used for the fit. With OTB the B2 and $B_h$ phases for TiC and the B2 phase for TiN are more stable compared to the *ab initio* results, but still are well above the ground state. The full set of repulsive energy parameters for elemental and binary interactions is given in Table II. Two comments should be made regarding the binary compounds: (1) the repulsive embedding parameters for binaries are taken from the elemental values (e.g., carbon embedding parameters are used when the repulsive energy at a carbon site is estimated); and (2) local charge neutrality is imposed as an approximation to the self-consistent charge distribution.

## III. RESULTS AND DISCUSSION

The OTB models for Ti-C and Ti-N were constructed by fitting binding energy curves for various stoichiometric crystal structures. Therefore, it is important to test the applicability of these tight-binding models for different physical quantities and for atomic configurations with environments different from those considered in the fitting database. In this section, the performance of the present OTB models is compared with LDA and generalized-gradient-approximation (GGA) calculations, experiment, and existing tight-binding results.

At 1:1 composition, the total and projected densities of states of TiC and TiN structures are shown in Figs. 4 and 5. For all structures the bonding region shows a strong hybridization of C/N *p*- and Ti *d*-states, while the antibonding part is predominantly Ti *d* states with a small degree of hybridized C/N *p* states. Note that the decomposition of the DFT-DOS in these calculations is done by projection of the charge density onto orbitals within a PAW sphere and the sum of the projected *s*, *p*, and *d* contributions is typically 60% to 80%. The tight-binding models reproduce reasonably well the main features of the LDA-DOS. An exception is the B3 structure which is found to be metallic instead of semiconducting (i.e., the LDA band gap is not reproduced by the OTB models). This may also explain why the binding energy curve of the B3 structure shows one of the largest deviation from the LDA data (see Fig. 3) and may be related to the fact that the B3 phase has the largest separation between the first and second nearest neighbors (right panels of Figs. 4 and 5).

Compared to the Ti-C tight-binding model of Tan *et al.*,[26] which reported that the $B_h$ structure was only 0.39 eV/atom higher in energy than the B1 ground-state structure, we obtained a value of 0.53 eV/atom (see Fig. 3). Using the parameters of Ref. 26 we also find that the competing $B8_1$ structure is only 0.05 eV/atom above the ground state, whereas our present OTB model gives 0.27 eV/atom. The most serious flaw of the previous OTB model is the failure to properly describe structures away from equilibrium. For example, at equilibrium volume the B2 structure is 0.67 eV/atom above the ground state, but it becomes 2.0 eV/atom lower in energy than the ground state when the lattice constant is increased by 2%. This latter problem renders the model impractical and is a direct result of a too short cutoff distance adopted in the tail function for the Ti-C interaction.

To test the stability of our OTB models for short-distance C-C/N-N interactions, we have calculated the binding energy of $Ti_2C_2/Ti_2N_2$ compounds in the $Li_2C_2$ structure[63] made out of $C_2$ dimers immersed in the metal sublattice. The special treatment of the dimer interactions allows our models to correctly place the structure above the NaCl ground state: by 0.35 eV/atom for TiC (0.22 eV/atom in the LDA) and by 0.55 eV/atom for TiN (0.57 eV/atom in the LDA). For comparison, in the previous OTB model[26] the TiC structure is only 0.016 eV/atom above the ground state.

TABLE III. The elastic properties and phonon frequencies of TiC and TiN in the NaCl structure calculated with the present OTB models in comparison with DFT calculations, experimental data, and previous OTB results. The units of elastic constants and phonon frequencies are GPa and $cm^{-1}$, respectively.

| | OTB | OTB | LDA | GGA | Exp | | |
|---|---|---|---|---|---|---|---|
| TiC | | | | | | | |
| $C_{11}$ | 313[a] | 615 | 596 | 519 | 418[b] | 500[c] | 510[d] |
| $C_{44}$ | 119[a] | 140 | 177 | 183 | 217[b] | 175[c] | 180[d] |
| $C_{12}$ | 207[a] | 90 | 130 | 115 | 89[b] | 113[c] | 100[d] |
| $C_{11}-C_{12}$ | 106[a] | 525 | 466 | 404 | 329[b] | 387[c] | 410[d] |
| $C_{12}-C_{44}$ | 88[a] | −50 | −47 | −68 | −128[b] | −62[c] | −80[d] |
| $B$ | 243[a] | 265 | 285 | 250 | 241[b] | 242[c] | 237[d] |
| $\Gamma_{LTO}$ | | 584 | 555 | | 544[e] | | |
| $X_{TA}$ | | 306 | 303 | | 284[e] | | |
| $X_{LA}$ | | 352 | 378 | | 360[e] | | |
| $X_{TO}$ | | 569 | 552 | | 550[e] | | |
| $X_{LO}$ | | 606 | 614 | | 617[e] | | |
| $L_{TA}$ | | 309 | 278 | | 269[e] | | |
| $L_{LA}$ | | 469 | 470 | | 445[e] | | |
| $L_{TO}$ | | 621 | 597 | | 570[e] | | |
| $L_{LO}$ | | 740 | 746 | | 720[e] | | |
| TiN | | | | | | | |
| $C_{11}$ | | 740 | 710 | 579 | 498[f] | 507[g] | 631[h] |
| $C_{44}$ | | 157 | 177 | 180 | 168[f] | 163[g] | 170[h] |
| $C_{12}$ | | 130 | 135 | 129 | 106[f] | 96[g] | 171[h] |
| $C_{11}-C_{12}$ | | 610 | 575 | 450 | 392[f] | 411[g] | 460[h] |
| $C_{12}-C_{44}$ | | −27 | −42 | −51 | −62[f] | −67[g] | 1[h] |
| $B$ | | 333 | 326 | 279 | 237[f] | 292[g] | 320[h] |
| $\Gamma_{LTO}$ | | 645 | 553 | | 494[i] | | |
| $X_{TA}$ | | 309 | 271 | | 272[i] | | |
| $X_{LA}$ | | 416 | 322 | | 334[i] | | |
| $X_{TO}$ | | 554 | 560 | | 583[i] | | |
| $X_{LO}$ | | 580 | 583 | | 569[i] | | |
| $L_{TA}$ | | 304 | 206 | | 205[i] | | |
| $L_{LA}$ | | 471 | 278 | | 304[i] | | |
| $L_{TO}$ | | 562 | 566 | | 563[i] | | |
| $L_{LO}$ | | 575 | 623 | | 620[i] | | |

[a]Reference 26.
[b]Reference 69.
[c]Reference 70.
[d]Reference 71.
[e]Reference 66.
[f]Reference 72.
[g]Reference 73.
[h]Reference 74.
[i]Reference 67.

We have calculated the elastic and vibrational properties for TiC and TiN in the NaCl structure. The predicted elastic constants are in very good agreement with the DFT and experimental values, and show a distinct improvement over the model of Ref. 26 (see Table III). In particular, our OTB models reproduce the negative Cauchy pressure, a quantity known to be notoriously hard to predict within the tight-binding approximation for environmentally independent repulsive potentials.[61,62,64] The phonon dispersions were calculated with the frozen phonon method as implemented in PHON[65] using sufficiently large ($4 \times 4 \times 4$) supercells of the primitive two-atom NaCl unit cell to ensure the accurate evaluation of the dynamical matrix. The resulting $\omega(q)$ dependences along the high-symmetry directions in the Brillouin zone are shown in Fig. 6. For TiC, the agreement between the OTB and LDA results is impressive for all the acoustic and optical phonon modes. For TiN, the speed of sound of the transverse acoustic modes along $\Gamma$-$X$ in our OTB model is about half of that in the LDA and some phonon frequencies at the boundary of the Brillouin zone are up to 70% higher than those in the LDA. These results highlight the difficulty of describing the Ti-N system with a simple OTB model which does not explicitly includes the charge transfer. We would like to note that none of the elastic constants or vibrational frequencies were used in

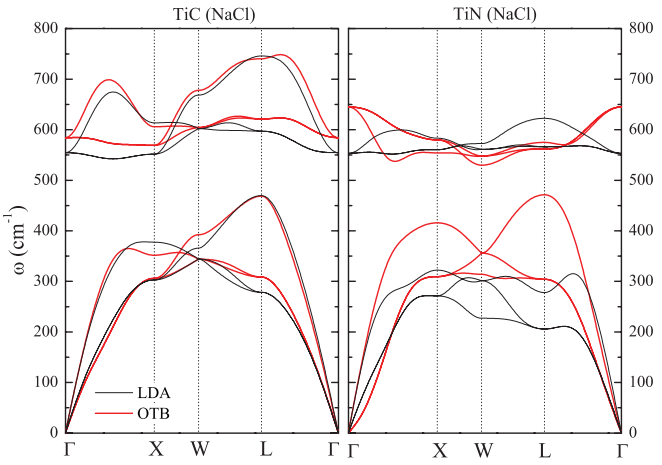


FIG. 6. (Color online) The phonon spectra for TiC and TiN in the NaCl structure calculated using the present OTB model (red lines) are compared with the LDA calculations (black lines).

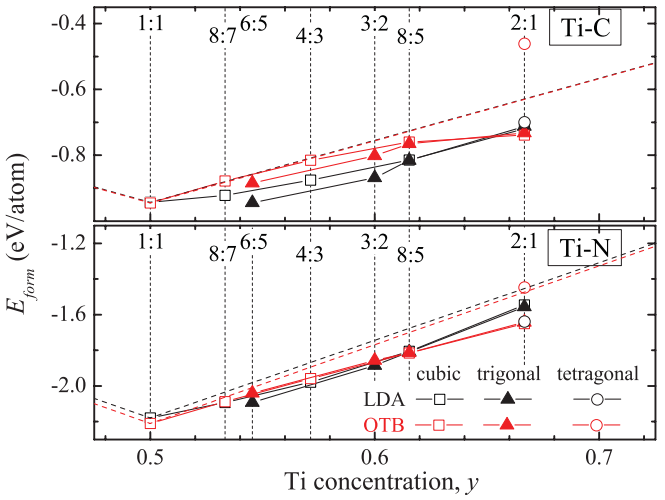


FIG. 7. (Color online) Calculated formation energy for vacancy-ordered structures in $Ti_yC_{1-y}$ (top) and $Ti_yN_{1-y}$ (bottom). The LDA and OTB values are shown in black and red, respectively. The dashed lines connect the binary ground state at 1:1 composition to the elemental ground states.

the fitting process, and the generally good agreement with the relevant DFT values can serve as an indication of an improved transferability of our models.

As a final transferability test of the presented OTB models, we investigate the formation energy of vacancy-ordered structures in the substoichiometric Ti-C and Ti-N compounds. To describe the formation energy we use the $Ti_yX_{1-y}$ ($X$ = C or N) notation for nonmetal deficient titanium nitride and titanium carbide phases. The nonmetal concentration is denoted as $1-y$ instead of $x$ to avoid confusion with the alternative notation $TiX_x$, where $[y = 1/(1+x)]$. The formation energy is evaluated relative to the energies of pure elements in their ground-state structures. The formation energy per atom for $Ti_yX_{1-y}$ ($X$ = C or N) is given by the following equation:

$$E_{\text{form}} = E(\text{Ti}_y X_{1-y}) - yE(\text{Ti}) - (1-y)E(X), \qquad (7)$$

where $E(Ti_yX_{1-y})$ is the total energy per atom for $Ti_yC_{1-y}$ or $Ti_yN_{1-y}$ binary, $E$(Ti) is the total energy per atom for titanium in the hexagonal close-packed structure, and $E(X)$ is the total energy per atom for nonmetal $X$ (graphite structure for carbon and $N_2$ molecule for nitrogen).

To study the cubic phase at several stoichiometries, from $y = 0.5$ (1:1 Ti to $X$ ratio) to 0.667 (2:1 Ti to $X$ ratio), a $2 \times 2 \times 2$ supercell with an fcc lattice and a basis of eight titanium and eight carbon/nitrogen atoms was used. One up to four nonmental atoms were subsequently removed to create $Ti_8X_7$ ($y = 0.533$), $Ti_8X_6$ ($y = 0.571$), $Ti_8X_5$ ($y = 0.615$), and $Ti_8X_4$ ($y = 0.667$) structures as described in Ref. 17. Since for $y = 0.571$ and $y = 0.615$ two combinations of vacancies are possible, we have chosen the configurations with the lowest formation energies.[17] In addition to the cubic phase, we examined four substoichiometric trigonal phases,[8,18,68] $Ti_8X_5$ ($y = 0.615$), $Ti_6X_5$ ($y = 0.545$), $Ti_3X_2$ ($y = 0.6$), and $Ti_4X_2$ ($y = 0.667$), and one substoichiometric tetragonal phase[8] $Ti_3X_2$ ($y = 0.667$). Relaxation of these structures in the LDA and OTB models involved optimization of both the lattice vectors and the internal atomic coordinates. The formation energy as a function of the titanium concentration for all studied phases are shown in Fig. 7.

From the upper panel of Fig. 7 we can see that for the TiC system, the OTB model predicts the cubic-based vacancy structure to be slightly lower in energy than the trigonal-based one at 2:1 composition. As the carbon content is increased and the vacancies are gradually filled, the relative order is interchanged and the trigonal-based structures become the most stable. This finding is consistent with the cubic-to-trigonal transition found within our LDA calculations and reported previously in a Monte Carlo study.[18]

For the TiN system similar formation energies as for TiC are obtained with the current tight-binding model (see the low panel of Fig. 7). However, this is not consistent with the LDA calculations at 2:1 composition that predicts the tetragonal phase to be the ground state. Even though the relative energy difference between the cubic and tetragonal structures is slightly reduced in TiN as compared to TiC, the energy decrease of 0.08 eV/atom is insufficient to stabilize the tetragonal phase that remains 0.2 eV/atom above the estimated cubic ground state. We have carried out further calculations to clarify the energy difference between the cubic and tetragonal structures. By adjusting the volume of the tetragonal phase to give the same repulsion energy as for the cubic one, we estimated a bond energy difference between them of 0.2 eV/atom. This indicates that the mismatch between their formation energies is predominantly due to the bond term. A better description of the subtle formation energy differences in the off-stoichiometric Ti-C and Ti-N compounds may require the introduction of environment-dependent bond integrals and an explicit treatment of the charge transfer.

## IV. SUMMARY AND CONCLUSION

In this study we present a systematic approach for the parametrization of orthogonal tight-binding models for titanium carbide and nitride compounds directly from density functional theory calculations. The development procedure involves two successive steps: (i) the bond integrals are

extracted from the projection of one-electron wave functions (from well-converged plane-wave-based DFT calculations) onto a basis of shape- and range-optimized atom-centered orbitals (by means of a recently developed method[50]), and (ii) the repulsive potential is constructed by fitting DFT binding energy versus volume curves. By introducing a core correction term for C and N, we are able to fix the short-range behavior of the potential for the dimer and obtain a reasonable description of their elemental phases despite the incompleteness of the *p* orbital basis set. To describe the Ti-Ti interaction we use the standard tight-binding approximation for transition metals that includes only the *d* states and choose the same *d*-band filling for the unary and binary phases. Although more accurate TB parametrizations exist for the pure Ti and C/N systems, the use of single sets of composition-independent parameters in the proposed OTB *pd* models lifts the restriction on the simulation of only specific compositions. Overall, our simple *pd* OTB models are able to provide a fairly accurate description of the density of states, binding energies, formation energies, elastic constants, and vibrational properties of bulk Ti-C and Ti-N phases over a wide range of stoichiometries.

## ACKNOWLEDGMENTS

E.R.M. and A.N.K. acknowledge the support of the EPSRC through Grant Nos. EP/E065902/1 and CAFEP/G004072/1. M.R., M.M., and C.E. acknowledge the support by the German Research Foundation (DFG) via Grants No. MR 22/5-1,2, by the German Ministry of Education and Research (BMBF) via Grant No. 03X0511, and by European Commission through Contract No. NMP.2010.2.5-1.263335 (MultiHy). B.M. acknowledges the support by the DFG via Grants No. ME 2670/3-1,2.

## APPENDIX

A core correction term is added "ad hoc" to the repulsive energy at small distances in the case of carbon and nitrogen to describe the $C_2$ and $N_2$ molecules. This term takes the following form:

$$U_{\text{core}} = \sum_i \sum_j C_i(r_{ij})\, \alpha e^{-\lambda(r_{ij}-R_0)} T(r_{ij}),$$

where $T(r_{ij})$ and $C_i(r_{ij})$ are the tail cutoff function and the coordination number of atom $i$. $T(r_{ij})$ is expressed as

$$T(r_{ij}) = \begin{cases} 1, & 0 < r_{ij} < R_1, \\ \frac{1}{2}\left\{1 + \cos\left[\frac{\pi(r_{ij}-R_1)}{R_2-R_1}\right]\right\}, & R_1 < r_{ij} < R_2. \end{cases}$$

The coordination number is estimated by counting all the neighbors within a specific radius

$$C_i(r_{ij}) = \begin{cases} 1, & Z_i(r_{ij}) < Z_1, \\ \frac{1}{2}\left\{1 + \cos\left[\frac{\pi(Z_i(r_{ij})-Z_1)}{Z_2-Z_1}\right]\right\}, & Z_1 < Z_i(r_{ij}) < Z_2, \end{cases}$$

where

$$Z_i(r_{ij}) = \begin{cases} \sum_j 1, & 0 < r_{ij} < R_2, \\ \sum_j \frac{1}{2}\left\{1 + \cos\left[\frac{\pi(r_{ij}-R_2)}{R_3-R_2}\right]\right\}, & R_2 < r_{ij} < R_3. \end{cases}$$

In this study we have used the following values for the tail cutoff function and the coordination number: $R_0 = 1.25$ Å, $R_1 = 1.6$ Å, $R_2 = 1.8$ Å, $R_3 = 2.0$ Å, $Z_1 = 1.0$, and $Z_2 = 1.1$. The values for $\alpha$ and $\lambda$ were 6.964 (−0.908) and 1.220 (0.028) for carbon (nitrogen).

[1] H. O. Pierson, *Handbook of Refractory Carbides and Nitrides: Properties, Characteristics, Processing, and Applications* (Noyes Publications, Bracknell, England, 1996).
[2] *The Physics and Chemistry of Carbides, Nitrides, and Borides*, edited by R. Freer (Kluwer, Dordrecht, 1990).
[3] J. Musil, Surf. Coat. Technol. **125**, 322 (2000).
[4] S. Veprek, M. G. J. Veprek-Heijman, P. Karvankova, and J. Prochazka, Thin Solid Films **476**, 1 (2005).
[5] S. Veprek and M. J. G. Veprek-Heijman, Surf. Coat. Technol. **202**, 5063 (2008).
[6] H. C. Barshilia, M. S. Prakash, D. V. S. Rao, and K. S. Rajam, Surf. Coat. Technol. **195**, 147 (2005).
[7] D. Martínez-Martínez, C. López-Cartes, A. Justo, A. Fernández, and J. C. Saánchez-López, Solid State Sci. **11**, 660 (2009).
[8] R. Eibler, J. Phys. Condens. Matter **19**, 196226 (2007) and references therein.
[9] H. Höchst, R. D. Bringans, P. Steiner, and T. Wolf, Phys. Rev. B **25**, 7183 (1982).
[10] M. Guemmaz, G. Moraitis, A. Mosser, M. A. Khan, and J. C. Parlebas, J. Phys. Condens. Matter **9**, 8453 (1997).
[11] M. Guemmaz, G. Moraitis, A. Mosser, M. A. Khan, and J. C. Parlebas, J. Electr. Spectr. Rel. Phenom. **83**, 173 (1997).
[12] M. Guemmaz, A. Mosser, and J. C. Parlebas, J. Electron Spectrosc. Relat. Phenom. **107**, 91 (2000).
[13] I. Pollini, A. Mosser, and J. C. Parlebas, Phys. Rep. **355**, 1 (2001).
[14] A. Dunand, H. D. Flack, and K. Yvon, Phys. Rev. B **31**, 2299 (1985).
[15] D. L. Price and B. R. Cooper, Phys. Rev. B **39**, 4945 (1989).
[16] M. Tsujimoto, H. Kurata, T. Nemoto, S. Isoda, S. Terada, and K. Kaji, J. Electron Spectrosc. Relat. Phenom. **143**, 159 (2005).
[17] H. W. Hugosson, P. Korzhavyi, U. Jansson, B. Johansson, and O. Eriksson, Phys. Rev. B **63**, 165116 (2001).
[18] P. A. Korzhavyi, L. V. Pourovskii, H. W. Hugosson, A. V. Ruban, and B. Johansson, Phys. Rev. Lett. **88**, 015505 (2001).
[19] Z. Dridi, B. Bouhafs, P. Ruterana, and H. Aourag, J. Phys. Condens. Matter **14**, 10237 (2002).
[20] A. Zaoui, S. Kacimi, B. Bouhafs, and A. Roula, Physica B **358**, 63 (2005).
[21] L. Tsetseris, N. Kalfagiannis, S. Logothetidis, and S. T. Pantelides, Phys. Rev. Lett. **99**, 125503 (2007); Phys. Rev. B **76**, 224107 (2007).
[22] L. Tsetseris and S. T. Pantelides, Acta Mater. **56**, 2864 (2008).
[23] Y. Yang, H. Lu., C. Yu, and J. M. Chen, J. Alloys Compd. **485**, 542 (2009).
[24] P. Marksteiner, P. Weinberger, A. Neckel, R. Zeller, and P. H. Dederichs, Phys. Rev. B **33**, 812 (1986).

[25]J. P. Landesman, G. Tréglia, P. Turchi, and F. Ducastelle, J. Phys. **46**, 1001 (1985).
[26]K. E. Tan, A. M. Bratkovsky, R. M. Harris, A. P. Horsfield, D. Nguyen-Manh, D. G. Pettifor, and A. P. Sutton, Modell. Simul. Mater. Sci. Eng. **5**, 187 (1997).
[27]J. Klima, J. Phys. C **12**, 3691 (1979).
[28]V. I. Ivashchenko, P. E. A. Turchi, V. I. Shevchenko, L. A. Ivashchenko, and O. K. Porada, Condens. Matter Phys. **7**, 79 (2004).
[29]Y.-M. Kim and B.-J. Lee, Acta Mater. **56**, 3481 (2008).
[30]M. Marlo and V. Milman, Phys. Rev. B **62**, 2899 (2000).
[31]A. T. Paxton, M. van Schilfgaarde, M. MacKenzie, and A. J. Craven, J. Phys. Condens. Matter **12**, 729 (2000).
[32]A. J. Scott, R. Brydson, M. MacKenzie, and A. J. Craven, Phys. Rev. B **63**, 245105 (2001).
[33]P. Patsalas and S. Logothetidis, J. Appl. Phys. **90**, 4725 (2001).
[34]P. Patsalas, C. Gravalidis, and S. Logothetidis, J. Appl. Phys. **96**, 6234 (2004).
[35]P. A. P. Lindberg, L. I. Johansson, J. B. Lindström, and D. S. L. Law, Phys. Rev. B **36**, 939 (1987).
[36]B. W. Karr, D. G. Cahill, I. Petrov, and J. E. Greene, Phys. Rev. B **61**, 16137 (2000).
[37]D. Gall, S. Kodambaka, M. A. Wall, I. Petrov, and J. E. Greene, J. Appl. Phys. **93**, 9086 (2003).
[38]K. Kobayashi, Jpn. J. Appl. Phys. **39**, 4311 (2000).
[39]K. Kobayashi, Surf. Sci. **493**, 665 (2001).
[40]R. F. Zhang, A. S. Argon, and S. Veprek, Phys. Rev. B **81**, 245418 (2010).
[41]X. J. Hu and Y. G. Shen, Appl. Phys. Lett. **94**, 093111 (2009).
[42]S. Hao, B. Delley, S. Veprek, and C. Stampfl, Phys. Rev. Lett. **97**, 086102 (2006).
[43]S. V. Dudiy and B. I. Lundqvist, Phys. Rev. B **69**, 125421 (2004).
[44]K. E. Tan, A. P. Horsfield, D. N. Manh, D. G. Pettifor, and A. P. Sutton, Phys. Rev. Lett. **76**, 90 (1996).
[45]R. M. Harris and P. D. Bristowe, Philos. Mag. A **79**, 705 (1999).
[46]D. G. Pettifor and R. Podloucky, J. Phys. C **19**, 315 (1986).
[47]H. Amara, J. M. Roussel, C. Bichara, J. P. Gaspard, and F. Ducastelle, Phys. Rev. B **79**, 014109 (2009).
[48]R. Drautz, X. W. Zhou, D. A. Murdick, B. Gillespie, H. N. G. Wadley, and D. G. Pettifor, Prog. Mater. Sci. **52**, 196 (2007) and references therein.
[49]A. P. Sutton, M. W. Finnis, D. G. Pettifor, and Y. Ohta, J. Phys. C **21**, 35 (1988).
[50]A. Urban, M. Reese, M. Mrovec, C. Elsässer, and B. Meyer, Phys. Rev. B **84**, 155119 (2011).
[51]L. Goodwin, A. J. Skinner, and D. G. Pettifor, Europhys. Lett. **9**, 701 (1989).
[52]C. H. Xu, C. Z. Wang, C. T. Chan, and K. M. Ho, J. Phys. Condens. Matter **4**, 6047 (1992).
[53]P. E. Blöchl, Phys. Rev. B **50**, 17953 (1994).
[54]J. P. Perdew and A. Zunger, Phys. Rev. B **23**, 5048 (1981).
[55]G. Kresse and J. Hafner, Phys. Rev. B **47**, 558 (1993); G. Kresse and J. Furthmüller, *ibid*. **54**, 11169 (1996).
[56]J. D. Pack and H. J. Monkhorst, Phys. Rev. B **13**, 5188 (1976); **16**, 1748 (1977).
[57]D. R. Trinkle, M. D. Jones, R. G. Hennig, S. P. Rudin, R. C. Albers, and J. W. Wilkins, Phys. Rev. B **73**, 094123 (2006).
[58]C. Mailhiot, L. H. Yang, and A. K. McMahan, Phys. Rev. B **46**, 14419 (1992).
[59]X. Wang, F. Tian, L. Wang, T. Cui, B. Liu, and G. Zou, J. Chem. Phys. **132**, 024502 (2010).
[60]D. G. Pettifor and R. Podloucky, Phys. Rev. Lett. **53**, 1080 (1984).
[61]A. Girshick, A. M. Bratkovsky, D. G. Pettifor, and V. Vitek, Philos. Mag. A **77**, 981 (1998).
[62]S. Znam, D. Nguyen-Manh, D. G. Pettifor, and V. Vitek, Philos. Mag. A **83**, 415 (2003).
[63]U. Ruschewitz and R. Pöttgen, Z. Anorg. Allg. Chem. **625**, 1599 (1999).
[64]D. Nguyen-Mahn, D. G. Pettifor, S. Znam, and V. Vitek, Mater. Res. Soc. Symp. Proc. **491**, 353 (1998).
[65]D. Alfè, Comput. Phys. Commun. **180**, 2622 (2009).
[66]L. Pintschovius, W. Reichardt, and B. Scheerer, J. Phys. C **11**, 1557 (1978).
[67]W. Kress, P. Roedhammer, H. Bilz, W. D. Teuchert, and A. N. Christensen, Phys. Rev. B **17**, 111 (1978).
[68]G. Bergerhoff and I. D. Brown, in *Crystallographic Databases*, edited by F. H. Allen *et al*. (International Union of Crystallography, Chester, England, 1987).
[69]Y. Kumashiro, H. Tokumoto, E. Sakuma, and A. Itoh, in *Proceedings of the Sixth International Conference on Internal Friction and Ultrasonic Attenuation in Solids* (Tokyo University Press, Tokyo, 1977), p. 395.
[70]J. J. Gilman and B. W. Roberts, J. Appl. Phys. **32**, 1405 (1961).
[71]W. Weber, Phys. Rev. B **8**, 5082 (1973).
[72]D. S. Rickerby, A. M. Jones, and B. A. Bellamy, Surf. Coat. Technol. **36**, 661 (1988).
[73]W. J. Meng and G. L. Eesley, Thin Solid Films **271**, 108 (1995).
[74]V. P. Zhukov, V. A. Gubanov, O. Jepsen, N. E. Christensen, and O. K. Andersen, J. Phys. Chem. Solids **49**, 841 (1988).